










Direct measurement of delayed-detachment rate constants of C_7^- S. Iida ^{1,*}, S. Kuma ², J. W. Niman ³, S. Masuda ¹, H. Tanuma ¹, P. Ferrari ⁴, K. Hansen ^{5,6},
H. Shiromaru ¹ and T. Azuma ^{2,1}¹*Department of Physics, Tokyo Metropolitan University, Hachioji, Tokyo 192-0397, Japan*²*Atomic, Molecular and Optical Physics Laboratory, RIKEN, Wako, Saitama 351-0198, Japan*³*Department of Physics and Astronomy, University of Southern California, Los Angeles, California 90089-0484, USA*⁴*Radboud University, Institute for Molecules and Materials, HFML-FELIX, 6525 ED Nijmegen, Netherlands*⁵*Center for Joint Quantum Studies and Department of Physics, School of Science, Tianjin University, Tianjin 300072, China*⁶*Lanzhou Center for Theoretical Physics, Key Laboratory of Theoretical Physics of Gansu Province, Lanzhou University, Lanzhou, Gansu 730000, China*

(Received 28 August 2023; accepted 21 November 2023; published 11 December 2023)

Delayed electron detachment induced by resonant two-photon excitation of C_7^- is observed using an electrostatic ion storage ring. Radiative cooling during the period of more than 100 ms storage considerably narrows the initially very broad internal energy distributions resulting in the delayed detachment profiles to be well fitted by single-exponential functions. The time constants of the decay, representing the electron detachment rate constants, are found to be much smaller than the theoretically predicted ones based on the detailed balance theory employing the state density of the harmonic vibrations.

DOI: [10.1103/PhysRevA.108.062808](https://doi.org/10.1103/PhysRevA.108.062808)**I. INTRODUCTION**

Small carbon cluster anions, of which chain-form structures are most stable, are considered promising candidates for interstellar molecular anions, especially since findings of hydrogen-terminated carbon chain anions in space [1,2]. Compared with both neutrals and molecular cations, anions are, in general, fragile because of their much lower threshold for thermal decay. The survival probability of anions excited to an energy level above the electron detachment threshold is determined by a competition between spontaneous electron detachment (autodetachment) and stabilization by radiative cooling. This potentially increases the survival rate by a significant amount. Evaluation of these rates as a function of the internal energy is therefore of great importance to understand the stability of anions isolated in vacuum. Ion storage experiments on small carbon cluster anions conducted during the previous decade have already significantly deepened the understanding of radiative cooling, demonstrating that C_4^- and C_6^- are cooled by recurrent fluorescence whereas C_5^- and C_7^- are cooled solely by vibrational transitions [3–8].

On the other hand, the evaluation of electron detachment rates, as a function of the internal energy, has relied on theoretical calculations because of the lack of experimental values. Autodetachment is a thermal process of highly excited molecules for which treatments by first-principle calculations are difficult. The missing ingredients are precise level densities and electron attachment cross sections for the neutral. The effects associated with angular momentum conservation, briefly discussed at the end of this paper, add

to the theoretical uncertainty and allow some tolerance in the detachment rate constants derived by standard methods [9]. Thus, experimental determination of the rate constants, together with refinement of the theoretical procedure, will significantly enhance the reliability of the prediction of the survival probability of anions. In addition, accurate values of the detachment rate will improve estimates of the radiative cooling rate (see below), although this effect will admittedly be small.

In a previous paper on storage ring experiments of C_7^- , with storage times up to 35 ms, we showed that the reduction of the internal energies by vibrational radiative cooling can be tracked by a variation of the delayed electron detachment yields against the laser firing times (\simeq ion storage times) [4]. The analysis was based on the fact that the neutrals produced by photoexcitation are detected only for decays during a limited time window, specifically when electron detachment occurs in the straight section upstream of the detector during one of the revolutions of the ions in the ring. The counts of the detected neutrals are proportional to the number of the ions undergoing electron detachment during the time they spend in this straight section (time window). Considering the detachment rate constant as a function of the internal energy, the time windows were converted to the energy windows, of which the width strongly depends on the cluster size [3,5,7]. Recently, the vibrational radiative cooling rates of C_7^- were modeled in a time range up to several tens of seconds to reproduce the variation of the detachment yields measured in a cryogenic ion storage ring [10]. In these studies, the theoretically obtained detachment rate constants, calculated based on the detailed balance theory [11], were adopted.

In the present study, we revisit the question by measuring laser-induced delayed electron detachment from C_7^- stored

*s-iida@tmu.ac.jp

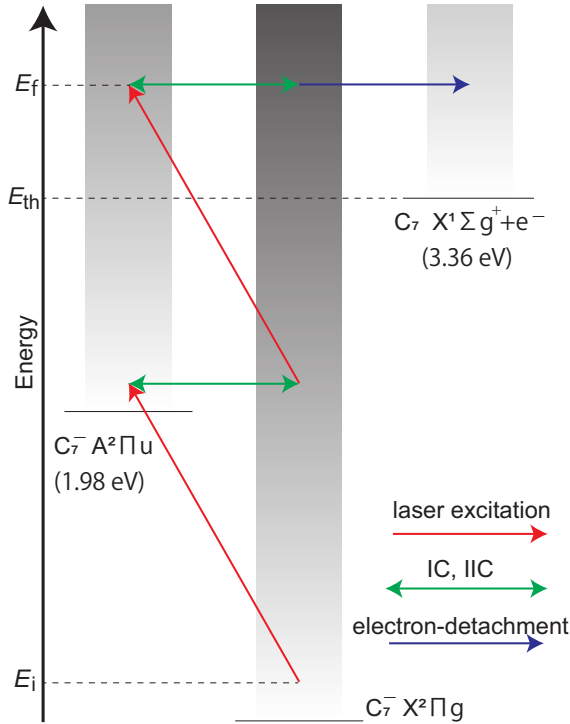


FIG. 1. Energy level diagram of C_7^- showing the electron detachment threshold E_{th} along with the X and A states. E_i is the internal energy before photoexcitation and E_f is the internal energy after two-photon excitation.

in an electrostatic storage ring (TMU E-ring), with laser firing times of up to 290 ms, combined with excitation spectroscopy by resonant one-color two-photon (1C2P) excitation. As a consequence of the longer storage times compared to our previous work, ions cool down further, leading to a narrower energy distribution of the internal energies. We will show that the electron detachment rate constants can be obtained experimentally as a function of the internal energy, with only a small uncertainty given by the internal energies before laser excitation.

A schematic energy diagram pertaining to the present study is shown in Fig. 1. The first step is excitation to the A state from the vibrationally excited X state with the internal energy denoted by E_i , from which the cluster gradually loses vibrational energy by radiation during storage. The band origin of the transition to the A state is determined to be 1.98 eV [12]. The second photon absorbed from the same laser shot, thus with the same wavelength, generates anions above the detachment threshold, providing the energy needed for delayed electron detachment. Within the time resolution of the ion storage experiments, internal conversion (IC), inverse internal conversion (IIC), and intramolecular vibrational energy redistribution (IVR) processes take place so rapidly that we can adopt a statistical model to treat these excited states as populated thermally by the vibrationally excited ions. That is, the electron detachment rate is governed by E_f , the energy of the emitting state, independently of the energy of the intermediate A state.

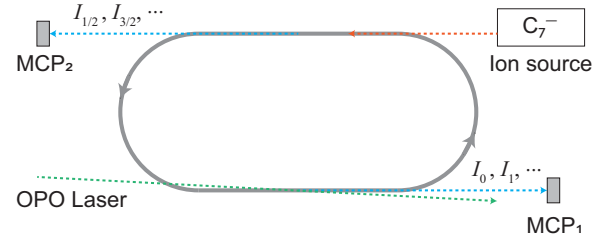


FIG. 2. Schematic drawing of the ion storage experimental setup. Stored C_7^- ions were photoexcited by the OPO laser beam which intersected the anion beam at a small angle to avoid hitting the MCP1, which detected the neutral species generated in the lower straight section. The neutral species generated in the upper straight section were detected with the MCP2. $I_{n/2}$ ($n = 0, 1, 2, \dots$) denote the signal intensity obtained at the $(n/2)^{\text{th}}$ revolutions after laser (see text).

As a typical chain-form cluster anion, the electronic and vibrational structures of C_7^- have been studied intensely both experimentally and theoretically [12–22]. The electron detachment threshold is determined to be 3.36 eV by photoelectron spectroscopy [14]. The electronic excitation of C_7^- has been studied by various methods, as summarized in the review paper of Ref. [23]. UV-vis absorption spectra of C_7^- embedded in the neon matrix present information on the transitions to the $A^2 \Pi$, $B^2 \Pi$, and $C^2 \Pi$ states with accompanying vibrational excitation of ν_1 , ν_2 , and ν_3 modes [17]. In the gas phase, an excitation spectrum of resonant multiphoton electron detachment from C_7^- shows several peaks assigned to transitions to the A state accompanying vibrational excitations [19]. Hot bands are observed in that spectrum, indicating that the anions are not entirely cooled by a helium carrier gas flow in the laser vaporization source. High-resolution excitation spectra obtained by two-color two-photon resonance enhanced detachment in which vibrational structures are well resolved and the close match of the peak positions to those of the diffuse interstellar bands (DIBs) are discussed in Refs. [12,20]. For C_7^- , photoexcitation results in electron detachment with no signature of dissociation [24], in contrast to the case of collision-induced reactions [25]. The vibrational spectroscopic constants of C_7^- have been obtained by IR absorption spectroscopy in argon matrix and theoretical calculations [18], which are also used in the present study.

II. EXPERIMENTS AND CALCULATIONS

The experimental setup is shown schematically in Fig. 2. The instrument has been described in detail in Ref. [26] to which the reader is referred for more details. Therefore, we just give a summary of the experiment here. Carbon cluster anions were produced by laser ablation of a graphite disk, irradiated by a 532-nm wavelength pulse from a Nd:YAG laser with a 10-Hz repetition rate. Cooling gases were not used in the source and the anions, therefore, retained considerable internal energies, as demonstrated in our previous work [3,5]. C_7^- anions were accelerated to 15 keV kinetic energy and injected into the TMU E-ring operated at room temperature, where C_7^- anions, composed only of the ^{12}C isotope, were mass-selected during storage by applying kick pulses;

at 100 μs storage anions with different numbers of carbons were removed by a first kick-pulse; at 400 μs storage, when the temporal separation of 84 and 85 amu became about 2 μs , hydrogen adduct anions and the ^{13}C containing anions were therefore removed by the second kick-pulse. An rf buncher was used to keep the bunch length shorter than 2 μs .

After a preset storage time, the ions were photoexcited with a wavelength-tunable nanosecond laser from an optical parametric oscillator (OPO), merged with the ion beam in one of the straight sections of the ring. The OPO laser power was fixed to 2.0 mJ/pulse, and the laser beam diameter was about 5 mm. The neutral particles produced by photoexcitation were detected using microchannel plate (MCP) detectors placed at the extension of the straight sections. Excitation spectra of $I_{n/2}$ ($n = 0, 1, 3, 5$), where $I_{n/2}$ stands for the yields at the $(n/2)^{\text{th}}$ revolutions after photoexcitation, were obtained by scanning the laser wavelength. As illustrated in Fig. 2, $n = 0$ corresponds to detachment in the laser merging side and odd numbers of n correspond to detachment in the opposite side. Hereafter, the delayed decay profiles are discussed for the odd integer values of n to avoid complications caused by the different detection efficiencies of the two detectors. The OPO wavelengths were scanned from 580 to 670 nm, covering transitions to the A state. Electron detachment yields by excitation wavelengths longer than 670 nm were very low, as expected. On the other hand, the delayed electron detachment was too fast to obtain the time constant of the decay when anions were excited with the wavelength shorter than 580 nm. The counts due to collision-induced detachment, evaluated by exponential fitting of the counts from 200 turns immediately before laser firing, were subtracted to obtain the true photon-induced detachment signal. The background signal due to autodetachment from the anions was evaluated from the yield without laser excitation, which was negligibly small in the relatively long storage time region of interest.

The procedure of the theoretical calculations of the emission rate constant is the same as that employed previously [8,27]. The electron detachment rate constant k_d for different internal energy E_f was calculated based on the principle of detailed balance theory [11] as follows:

$$k_d(E_f) = \int_0^{E-E_{\text{th}}} \frac{2m}{\pi^2 \hbar^3} \sigma_c(\epsilon) \epsilon \frac{\rho_d(E_f - E_{\text{th}} - \epsilon)}{\rho_p(E_f)} d\epsilon, \quad (1)$$

where m and ϵ are the mass and kinetic energy of the electron, respectively, and $\sigma_c(\epsilon)$ is the kinetic energy-dependent electron-capture cross section. $\sigma_c(\epsilon)$ was evaluated using the Langevin cross section $\pi e \sqrt{\frac{2\alpha}{4\pi\epsilon_0\epsilon}}$. The polarizability volume α was calculated to be 50.4 \AA^3 for the optimized geometry of the neutral molecule using the GAUSSIAN09 software [28]. The ρ_d and ρ_p are the level densities of the daughter (neutral) and parent (anionic) C_7 , respectively. The electronic degeneracies of the parent and daughter were included in their level densities and the spin degeneracy for the emitted electron is accounted for explicitly by the numerical factor of two in Eq. (1). The ρ_d and ρ_p were calculated numerically with the Beyer-Swinehart algorithm with the assumption that all the vibrations were harmonic. The quantum energies of the vibrations of the 16 modes of linear structures were adopted

from [18] for the anion and from [29] for the neutral. The effect of the Renner-Teller distortion on the number of vibrational degrees of freedom and the density of states is discussed below.

At a given internal energy E , the photon emission rate constant $k_v^{(i)}(E)$ of the vibrational transition for the i th vibrational mode is given by

$$k_v^{(i)}(E) = S_v A_{1-0}^{(i)} \frac{1}{\rho(E)} \sum_{n=1}^{E/h\nu_i} \rho(E - nh\nu_i), \quad (2)$$

where n is the vibrational quantum number, ν_i is the vibrational frequency of the i th mode, and ρ is the level density of all the vibrational modes of the anion. $A_{1-0}^{(i)}$ is the Einstein A coefficient for the vibrational transition i and S_v is a dimensionless fit parameter that corrects the calculated A coefficient, analogous to the procedure used in Refs. [8,27]. The electronic cooling rate is negligibly low (25 to 100 s^{-1}) for the relevant values of E_f .

For anions with high internal energies, radiative cooling of C_7^- was found to be dominated by a single vibrational mode, ν_5 with the numbering used in Ref. [18] (ν_{13} in Ref. [10]). For this mode the A coefficient is more than one order of magnitude larger than the others. Later, we approximate the total vibrational cooling rate $k_v(E)$ by $k_v^{(5)}(E)$ in the energy region where $k_v(E_f)$ and $k_d(E_f)$ compete. This convenient approximation is justified by the fact that averages of energy distributions cool exponentially with time, irrespective of the form of the distribution [30]. This means we can approximate the cooling with the dominant term with little error. What is required for this exponential decrease is a sufficiently fast statistical mixing, or intramolecular vibrational energy redistribution, and some amount of vibrational excitation energy.

III. RESULTS AND DISCUSSION

Excitation spectra of electron detachment observed at different revolutions after excitation are shown in Fig. 3, where the laser firing times (storage times) are 80 ms (left) and 190 ms (right). The peak at around 630 nm ($1h\nu = 1.97$ eV) (peak I) is assigned to the band origin of the transition to the A state, and that at around 605 nm ($1h\nu = 2.05$ eV) in the I_0 spectrum (peak II) corresponds to the transition to the vibrationally excited A state (3_0^1), referring to the reported spectra [19]. The broad band feature of these peaks are due to the overlap of many transitions, involving initially excited low-frequency modes and unresolved rotational envelopes.

The peak II becomes much lower in the $I_{1/2}$ spectrum and disappears in the spectra measured at later times, whereas the peak I remains. The faster decay of the peak II is interpreted simply as due to the higher E_f , which causes a faster depletion of the population. The I_0 spectrum obtained at 190 ms shows significant lowering of the signal intensity in the higher-energy region and resembles the spectrum of the ‘‘moderately hot’’ C_7^- measured previously, where anions produced by laser ablation of graphite with cooling gas were used soon after production [19]. As for the relative intensities of the spectra as a function of time after laser irradiation, a detailed discussion is provided below.

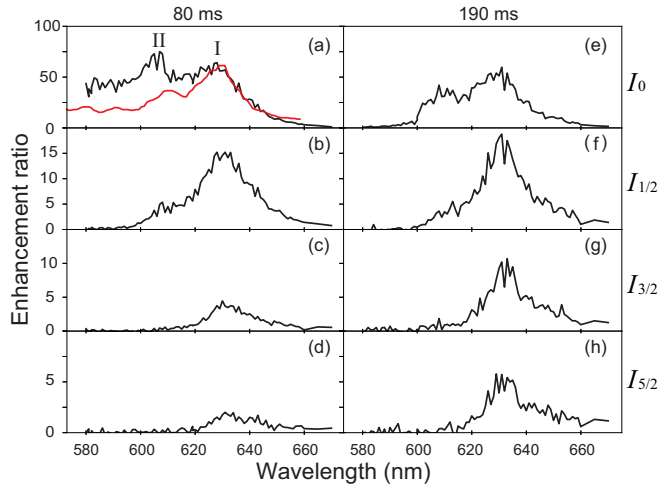


FIG. 3. Excitation spectra of (a) I_0 , (b) $I_{1/2}$, (c) $I_{3/2}$, (d) $I_{5/2}$ obtained at 80 ms and (e) I_0 , (f) $I_{1/2}$, (g) $I_{3/2}$, (h) $I_{5/2}$ 190 ms laser firing times. The vertical axis is the ratio of the laser-induced counts to the collision-induced counts. The spectrum depicted in the red line is a trace of that reported previously [19].

Plots of $I_{1/2}$ versus the laser firing times are shown in Fig. 4, where the excitation wavelengths are [Fig. 4(a)] 610 nm and [Fig. 4(b)] 640 nm. As seen from Fig. 3(a), 610-nm excitation corresponds to the higher-energy shoulder of the band I and 640-nm excitation corresponds to the hot band. The observed fast decrease of the signal, up to 20 ms, common for both spectra, is due to the decay of the high E_i components for which one-photon absorption induces electron detachment. After this initial decrease, the detachment yields slowly increase, reflecting an increase of the low-energy components, which are lifted to the region of slow electron detachment by two-photon absorption. Such switching from one- to two-photon processes was also observed for C_4^- and C_6^- [8]. At longer times the yields for 640-nm excitation [Fig. 4(b)] decrease again, corresponding to a decrease of the hot band

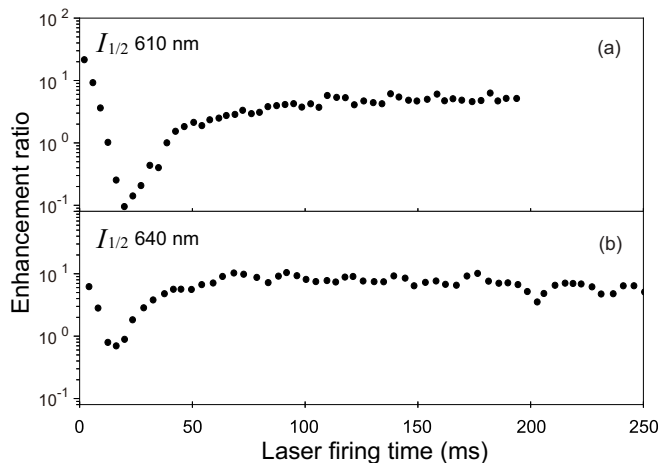


FIG. 4. Plots of the laser-induced electron detachment yields after $I_{1/2}$ turn in the ring versus laser firing times for (a) 610-nm excitation and (b) 640-nm excitation. The vertical axis is the ratio of the laser-induced counts to the collision-induced counts.

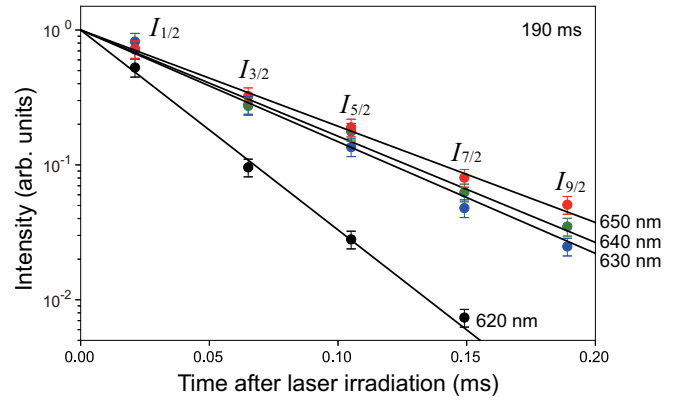


FIG. 5. Delayed detachment curves obtained at the laser firing time of 190 ms, with the wavelengths of 620, 630, 640, and 650 nm. The lines give the fits of single exponential functions to the decays. The intensities are here normalized to 1 for $t = 0$. Some part of the scatter around the lines is due to the betatron oscillations of the ion trajectories.

intensity. On the other hand, the yields for 610-nm excitation [Fig. 4(a)] appear to approach an asymptote, reflecting a slow increase of the population of near-ground states.

From the data shown in Figs. 3(e), 3(f), 3(g), and 3(h), we made the plots of $I_{n/2}$ with the excitation wavelengths of 620, 630, 640, and 650 nm ($2h\nu = 4.00, 3.94, 3.88, \text{ and } 3.82 \text{ eV}$) at a laser firing time of 190 ms, as shown in Fig. 5. It is clear that each decay can be fitted by a single exponential function. This is not the case for those obtained at earlier laser firing time because of the presence of decays with different time constants, as demonstrated later (in Fig. 8). A reasonable interpretation is that the radiative cooling efficiently narrows the internal energy distribution at 190 ms, permitting us to describe the decay with a single common detachment rate constant across the distribution. The decay profiles show a systematic variation of the time constants (decay rates) with the excitation wavelength.

The time constant in the signal decay can be approximated by the electron detachment rate (k_d) as long as the radiative quenching rate of the electron emitting state is appreciably smaller than k_d . The validity of this assumption is examined below, but we note already in advance here that if radiative cooling contributes to the decay of the signal, the observed rate constant provides an upper limit to the true value.

To evaluate E_i , the time evolution of the energy distribution was simulated. For simplicity, energy distributions at the time of ion extraction from the source were calculated as pertaining to canonical conditions. The results assuming an ion source temperature of 2000 K are shown in Fig. 6. Hereafter, we focus on the behavior at 190 ms, where the energy distribution is not sensitive to the correction factor S_v for the IR cooling rate because the population of the vibrational excited state of the dominant IR mode (1835.7 cm^{-1} , ν_5 in Ref. [18]) is, in any case, very low, as demonstrated by the simulation in Ref. [10]. For example, use of twice the IR cooling rate leads to a lowering of the peak position of the distribution by only 0.03 eV. The terminal energy content is likewise fairly insensitive to

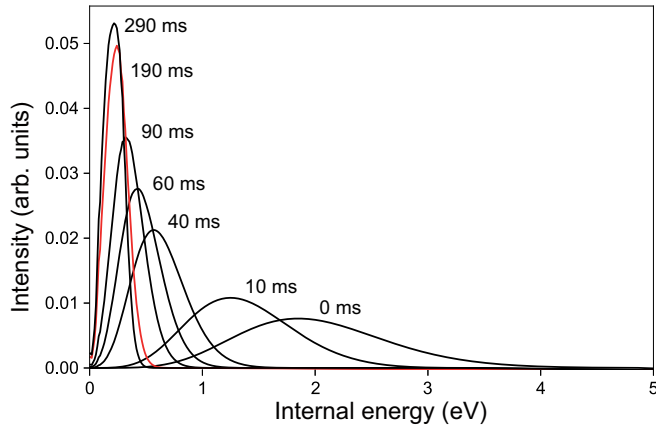


FIG. 6. Energy distributions of C_7^- simulated for various storage times, 0, 10, 40, 60, 90, 190, 290 ms (right to left) with the method described in Ref. [27]. The simulated distributions are smoothed for better visibility.

the value of k_d and to the initial ion source temperature. A change in these factors leads to a drastic change in the energy distributions at the beginning of ion storage, but the difference decreases with storage time. Thus, the nominal E_i values at 190 ms, ignoring the energy spread, can be safely estimated at 0.24 eV.

The procedure shown in Fig. 5 was applied to the data for all measured wavelengths. The obtained k_d is shown in Fig. 7 against the internal energy of electron-emitting anions, $E_f = 2h\nu + 0.24$ eV is shown in Fig. 7, together with the theoretically predicted k_d from Eq. (1). The k_d calculated with harmonic vibrations is about two orders of magnitude higher than the experimental k_d . The theoretical vibrational radiative cooling rates of the dominant IR mode ($k_v^{(5)} \simeq k_v$) are also indicated by the dashed red line, where the correction factor $S_v = 1$, determined by fitting the decay profiles as described below, is adopted. In the energy region surveyed in the present study, the condition $k_d \gg k_v$,

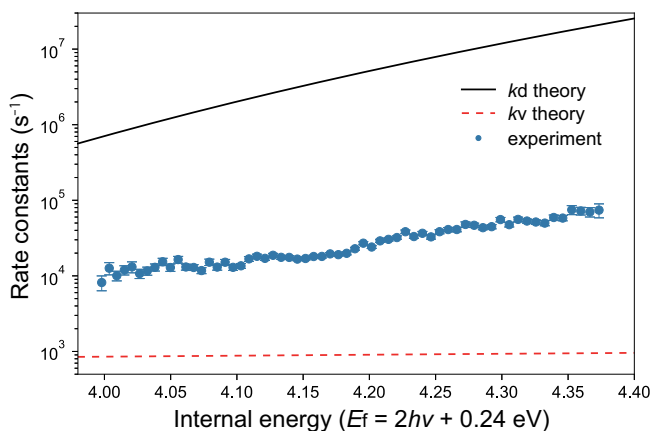


FIG. 7. Plot of k_d against E . The black line indicates the theoretical k_d obtained from the harmonic level densities and Eq. (1). The dashed red line indicates the vibrational photon emission rate constant of the main vibrational mode (k_v) calculated by Eq. (2).

required to approximate the measured decay rates with k_d , is satisfied.

To examine self-consistency, the decay profiles of shorter storage times, which are more sensitive to k_v , are simulated for $S_v = 0.5, 1.0, 2.0$ convoluting the k_d in Fig. 7 with the population in Fig. 6. The plots of $I_{n/2}$ obtained by varying laser firing times are shown in Fig. 8, for excitation wavelengths of 630, 640, and 650 nm. Simulated decay profiles are shown in solid lines, where slower decay corresponds to higher S_v . As a whole, good agreement is obtained for $S_v = 1$, which is adopted in the procedure of estimating E_i . The figure also demonstrates how the decay profiles approach a single exponential as cooling proceeds and become insensitive to S_v .

The long storage time which cools the ions to the low energies allows the comparison of the measured and theoretically obtained energy-resolved decay rate constant of the cluster without the complications caused by a broad excitation energy distribution and this is one of the strengths of this study. It is rather surprising that the experimental data show a rate constant reduced by about two orders of magnitude relative to the theoretical ones. Several candidates of the reason of this discrepancy are considered. One is the increased level densities calculated when anharmonicities are taken into account. The increase relative to the purely harmonic calculation affects the level density of the anion precursor ρ_p most strongly by the nature of the correction being second order in the quantum numbers.

Another potential effect that will affect the calculated rate constant is the conversion of a rotational degree of freedom of the anion to a vibrational mode for the neutral. The number of vibrational modes for the neutral is 16 due to its linear nature, whereas the Renner-Teller distortion reduces the number of modes of the anion to 15, that of a nonlinear molecule. This means that one rotational mode is converted into a vibrational mode upon electron emission. It is not obvious how to account for the energy in this conversion. Adding to the problem of the rotational-to-vibrational mode and energy conversion is the fact that vibrational modes in general carry angular momentum. See, for example, Ref. [22], where the special cases of linear molecules are considered. This entangles vibrational and rotational modes via both angular momentum and energy conservation during electron emission. It therefore also raises questions about the cross section for the reverse process of electron attachment to the neutral $\sigma_c(\epsilon)$. In the present study, the Langevin cross section derived from the theoretical polarizability, namely, that for the cold molecule at the equilibrium structure, was used for the estimate of the rate constant. This expression will overestimate the cross section if the energy dissipation in the collision is insufficient to take the electron kinetic energy below the electron affinity.

IV. CONCLUSION

We showed that the delayed electron detachment rates can be determined by resonance two-photon detachment of C_7^- after 190 ms of storage. The procedure will be applied in the future to other anions, for example, C_5^- , to elucidate the reason of the observed large difference between theoretical and experimental k_d values. Two-color two-photon detachment

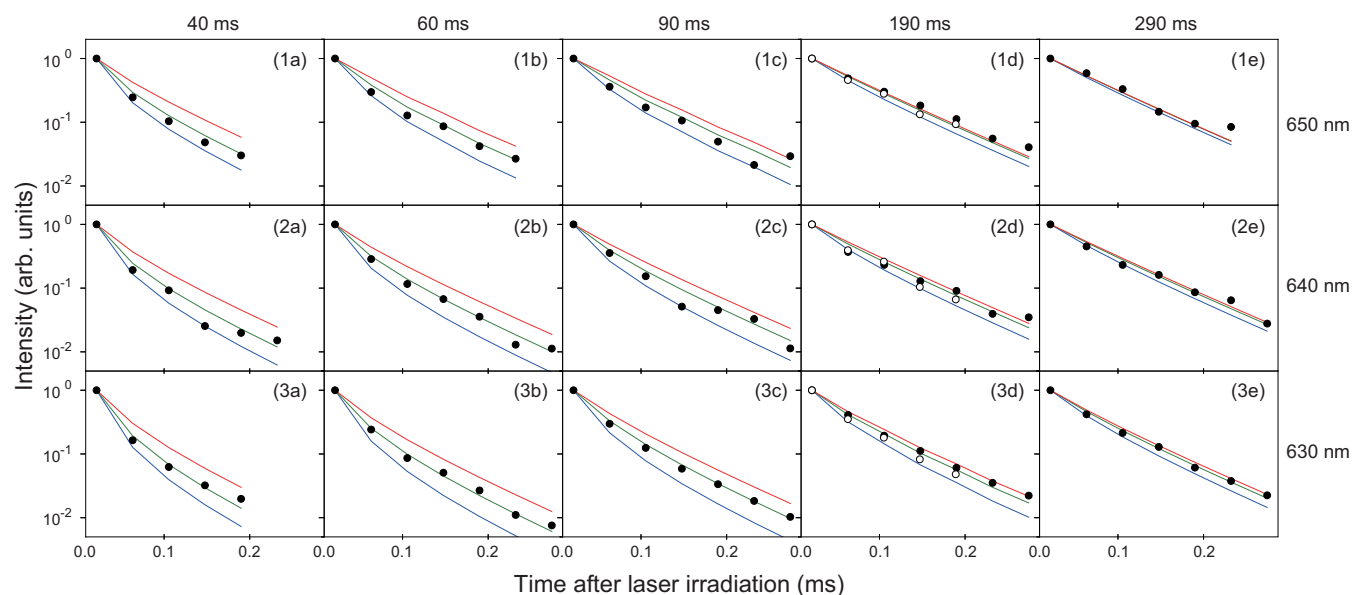


FIG. 8. Decay profile of the photodetachment yield of C_7^- induced by photoexcitation with the storage times of (a) 40, (b) 60, (c) 90, (d) 190, (e) 290 ms. The excitation wavelengths are (1) 650 nm, (2) 640 nm, (3) 630 nm. The open circles in (1d) to (3d) represent the decay profiles of independent runs shown in Fig. 5. The three lines in each frame indicate the decay profiles simulated with $S_v = 0.5, 1.0, 2.0$ (from lower to upper).

experiments are also planned to survey the detachment profiles near the electron detachment threshold. We found that the experimentally determined detachment rate constants are much lower than those derived by detailed balance theory together with the assumption that vibrations are harmonic. One reason for the overestimation in the theoretical values is that the harmonic oscillator approximation is invalid in regions of high vibrational energy. Another is specific to linear molecules: the difficulty in estimating the effect of conversion between rotational and vibrational modes. Angular momentum conservation should also be incorporated in the theory.

ACKNOWLEDGMENTS

This work was supported by the JSPS KAKENHI (Grant-in-Aid for Scientific Research (A) 21H04447, Grant-in-Aid for Early-Career Scientists 20K14386), the MEXT KAKENHI Grant No. 20H05848, the RIKEN Pioneering Projects, and with the Grant No. NSFC No. 12247101 and the U.S. National Science Foundation under Grant No. CHE-2153255 to JWN and the 111 Project under Grant No. B20063 from the Ministry of Science and Technology of People's Republic of China to KH.

- [1] A. Van Orden and R. J. Saykally, *Chem. Rev.* **98**, 2313 (1998).
 [2] T. J. Millar, C. Walsh, and T. A. Field, *Chem. Rev.* **117**, 1765 (2017).
 [3] M. Goto, A. Sundén, H. Shiromaru, J. Matsumoto, H. Tanuma, T. Azuma, and K. Hansen, *J. Chem. Phys.* **139**, 054306 (2013).
 [4] K. Najafian, M. S. Pettersson, B. Dynefors, H. Shiromaru, J. Matsumoto, H. Tanuma, T. Furukawa, T. Azuma, and K. Hansen, *J. Chem. Phys.* **140**, 104311 (2014).
 [5] G. Ito, T. Furukawa, H. Tanuma, J. Matsumoto, H. Shiromaru, T. Majima, M. Goto, T. Azuma, and K. Hansen, *Phys. Rev. Lett.* **112**, 183001 (2014).
 [6] V. Chandrasekaran, B. Kafle, A. Prabhakaran, O. Heber, M. Rappaport, H. Rubinstein, D. Schwalm, Y. Toker, and D. Zajfman, *J. Phys. Chem. Lett.* **5**, 4078 (2014).
 [7] N. Kono, T. Furukawa, H. Tanuma, J. Matsumoto, H. Shiromaru, T. Azuma, K. Najafian, M. S. Pettersson, B. Dynefors, and K. Hansen, *Phys. Chem. Chem. Phys.* **17**, 24732 (2015).
 [8] N. Kono, R. Suzuki, T. Furukawa, J. Matsumoto, H. Tanuma, H. Shiromaru, T. Azuma, and K. Hansen, *Phys. Rev. A* **98**, 063434 (2018).
 [9] K. Hansen, *Statistical Physics of Nanoparticles in the Gas Phase* (Springer, Dordrecht, The Netherlands, 2018).
 [10] M. H. Stockett, J. N. Bull, J. T. Buntine, E. Carrascosa, E. K. Andersson, M. Gatchell, M. Kaminska, R. F. Nascimento, H. Cederquist, H. T. Schmidt, and H. Zettergren, *Eur. Phys. J. D* **74**, 150 (2020).
 [11] J. U. Andersen, E. Bonderup, and K. Hansen, *J. Phys. B: At. Mol. Opt. Phys.* **35**, R1 (2002).
 [12] M. Tulej, D. A. Kirkwood, G. Maccaferri, O. Dopfer, and J. P. Maier, *Chem. Phys.* **228**, 293 (1998).
 [13] S. Yang, K. J. Taylor, M. J. Craycraft, J. Conceicao, C. L. Pettiette, O. Cheshnovsky, and R. E. Smalley, *Chem. Phys. Lett.* **144**, 431 (1988).
 [14] D. W. Arnold, S. E. Bradforth, T. N. Kitsopoulos, and D. M. Neumark, *J. Chem. Phys.* **95**, 8753 (1991).
 [15] H. Handschuh, G. Ganteför, B. Kessler, P. S. Bechthold, and W. Eberhardt, *Phys. Rev. Lett.* **74**, 1095 (1995).
 [16] S. Schmatz and P. Botschwina, *Int. J. Mass Spectrom. Ion Processes* **149-150**, 621 (1995).
 [17] D. Forney, M. Grutter, P. Freivogel, and J. P. Maier, *J. Phys. Chem. A* **101**, 5292 (1997).

- [18] J. Szczepanski, S. Ekern, and M. Vala, *J. Phys. Chem. A* **101**, 1841 (1997).
- [19] M. Ohara, H. Shiromaru, and Y. Achiba, *J. Chem. Phys.* **106**, 9992 (1997).
- [20] N. M. Lakin, M. Pachkov, M. Tulej, J. P. Maier, G. Chambaud, and P. Rosmus, *J. Chem. Phys.* **113**, 9586 (2000).
- [21] M. G. Giuffreda, M. S. Deleuze, and J.-P. François, *J. Phys. Chem. A* **106**, 8569 (2002).
- [22] K. Hansen and P. Ferrari, *Chem. Phys. Lett.* **768**, 138385 (2021).
- [23] J. P. Maier, *J. Phys. Chem. A* **102**, 3462 (1998).
- [24] B. Pozniak and R. C. Dunbar, *Int. J. Mass Spectrom. Ion Processes* **133**, 97 (1994).
- [25] S. W. McElvany, *Int. J. Mass Spectrom. Ion Processes* **102**, 81 (1990).
- [26] S. Jinno, T. Takao, K. Hanada, M. Goto, K. Okuno, H. Tanuma, T. Azuma, and H. Shiromaru, *Nucl. Instrum. Methods Phys. Res., Sect. A* **572**, 568 (2007).
- [27] S. Iida, S. Kuma, M. Kuriyama, T. Furukawa, M. Kusunoki, H. Tanuma, K. Hansen, H. Shiromaru, and T. Azuma, *Phys. Rev. A* **104**, 043114 (2021).
- [28] M. J. Frisch, G. W. Trucks, H. B. Schlegel, G. E. Scuseria, M. A. Robb, J. R. Cheeseman, G. Scalmani, V. Barone, B. Mennucci, G. A. Petersson *et al.*, *GAUSSIAN 09 Revision A.1*, Gaussian Inc. Wallingford, CT 2009.
- [29] H. Do and N. A. Besley, *Phys. Chem. Chem. Phys.* **17**, 3898 (2015).
- [30] K. Hansen, O. Licht, A. Kurbanov, and Y. Toker, *J. Phys. Chem. A* **127**, 2889 (2023).